

Modeling of complex oxide materials from the first principles: systematic applications to vanadates RVO_3 with distorted perovskite structure

Igor Solovyev

Received: date / Accepted: date

Abstract “Realistic modeling” is a new direction of electronic structure calculations, where the main emphasis is made on the construction of some effective low-energy model entirely within a first-principle framework. Ideally, it is a model in form, but with all the parameters derived rigorously, on the basis of first-principles electronic structure calculations. The method is especially suit for transition-metal oxides and other strongly correlated systems, whose electronic and magnetic properties are pre-determined by the behavior of some limited number of states located near the Fermi level. After reviewing general ideas of realistic modeling, we will illustrate abilities of this approach on the wide series of vanadates RVO_3 ($R=$ La, Ce, Pr, Nd, Sm, Gd, Tb, Yb, and Y) with distorted perovskite structure. Particular attention will be paid to computational tools, which can be used for microscopic analysis of different spin and orbital states in the partially filled t_{2g} -band. We will explicitly show how the lifting of the orbital degeneracy by the monoclinic distortion stabilizes C-type antiferromagnetic (AFM) state, which can be further transformed to the G-type AFM state by changing the crystal distortion from monoclinic to orthorhombic one. Two microscopic mechanisms of such a stabilization, associated with the one-electron crystal field and electron correlation interactions, are discussed. The flexibility of the orbital degrees of freedom is analyzed in terms of the magnetic-state dependence of interatomic magnetic interactions.

Keywords First-principle calculations · Effective models · Perovskite vanadates · Spin-orbital order

PACS 71.15.-m · 71.10.-w · 75.25.-j · 75.25.Dk

This work is partly supported by Grant-in-Aid for Scientific Research (C) No. 20540337 from the Ministry of Education, Culture, Sport, Science and Technology of Japan.

I. Solovyev
National Institute for Materials Science, 1-2-1 Sengen, Tsukuba, Ibaraki 305-0047, Japan
Tel.: +81-29-859-2619
Fax: +81-29-859-2601
E-mail: SOLOVYEV.Igor@nims.go.jp

1 Introduction

The transition-metal oxides are currently regarded as some promising materials for the future generation of electronic devices. The interest to these systems was spurred by the discoveries in them of such key phenomena as

1. high-temperature superconductivity (Cu- and Fe-based oxides) [1],
2. colossal magnetoresistance (doped manganites) [2],
3. multiferroelectricity (BiMnO₃, TbMnO₃) [3],

and many others, which can be potentially used in applications. One important aspect of the transition-metal oxides is realization of the so-called “switching phenomena”, where electronic properties can be controlled or easily switched between different states by various external factors, such as the hydrostatic pressure, electric or magnetic field, etc. For instance, the colossal magnetoresistance is the gigantic suppression of resistivity by the magnetic field, the multiferroelectricity provides a unique possibility for controlling the electric polarization by the magnetic field and vice versa, etc.

Besides the applications, there exists a long-standing fundamental interest to the transition-metal oxides, related to understanding of the above-mentioned phenomena on the microscopic level.

Historically, theoretical developments around the transition-metal oxides went almost parallel in two directions:

1. model approaches, based on the solution and analysis of all possible model Hamiltonians (the typical example is the Hubbard model, which is the basic and widely used model in the physics of strongly correlated systems) [4];
2. first-principles calculations, many of which are based on the density-functional theory (DFT) [5].

Each of these directions has merits and demerits. For example, the main advantage of the model analysis is the simplicity and transparency, while the main disadvantage is the use of adjustable parameters, which are typically chosen to fit the experimental data. On the contrary, the undisputable advantage of first-principles calculations is the lack of adjustable parameters. However, as calculations become more and more complex, we inevitably face the question about the interpretation of the obtained results. The problem is complicated by the fact that many first-principles methods are supplemented with some additional approximation for the exchange-correlation interactions. The most typical one is the local-density approximation (LDA), which is based on the model of homogeneous electron gas and undermines the physics of short-range Coulomb correlations. Thus, in the first-principles calculations for the transition-metal oxides we frequently face the question: are the obtained results physical or artifacts of additional approximations, which were employed in the process of calculations?

The primary goal of the new project, which is called “realistic modeling”, is the construction of “intelligent” models, which would combine the principles of simplicity and transparency with the rigorous first-principle basis for determination of the model parameters.

What is the main idea of realistic modeling?

Of course, the crystal and electronic structure of many oxide materials can be very complex. Nevertheless, as long as we are mainly concerned with electronic and magnetic properties of these systems, in many cases we can limit our consideration to a small group of states (the so-called low-energy states), which are located near the Fermi level

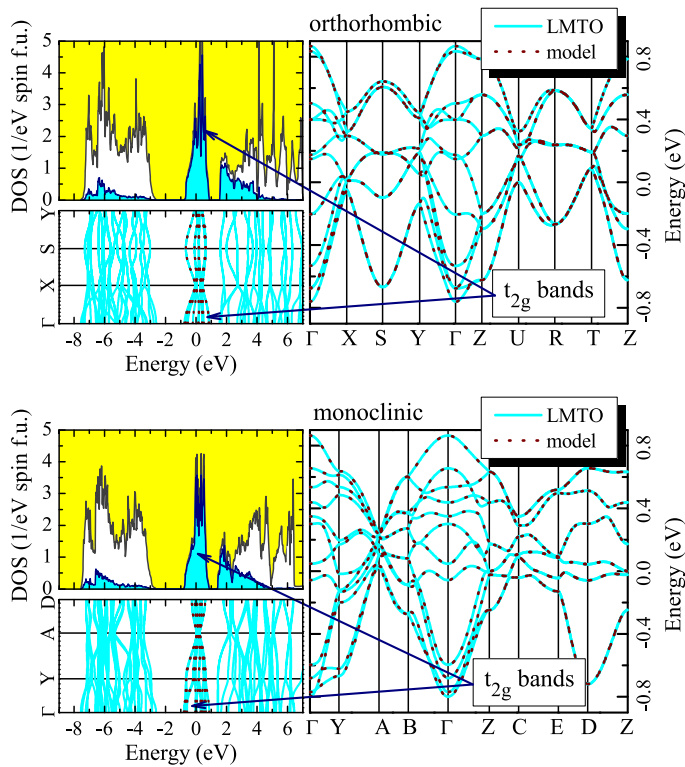


Fig. 1 Electronic structure for the orthorhombic (top) and monoclinic (bottom) phases of SmVO_3 in the local-density approximation. The shaded area shows the contributions of the V-3d states. Right part of the figure shows the enlarged behavior of the t_{2g} -bands computed from the original LMTO basis functions [6] (solid curves) and downfolded bands obtained in the process of construction of the low-energy model (dot-dashed curves). The corresponding bands in the left part of the figure are shown by arrows. The Fermi level is at zero energy.

and which are mainly responsible for the considered properties. The typical example of the LDA band structure of SmVO_3 is shown in Fig. 1. In this case, the low-energy states are the t_{2g} -bands. Thus, the main idea is to

1. construct an effective model for the low-energy states (typically, the multiorbital Hubbard model);
2. include the effect of all other states in some approximate form, through the definition of the model parameters for the low-energy states;
3. determine all model parameters rigorously, on the basis of first-principles calculations of the electronic structure.

What are the main goals of the realistic modeling?

1. It provides a possibility to go beyond the local-density approximation and to systematically study the effects of electron-electron correlations in the narrow bands. The solution of such a many-body problem is an extremely difficult task, even for the present computational facilities. Therefore, if there is a chance to formulate this problem rigorously in some *restricted* Hilbert space of states, near the Fermi level, there is a chance to solve it, at least numerically.

2. It is certainly true, that the first-principles calculations of the electronic structure are currently on the rise. However, as the complexity of such calculations also rises, we will inevitably need some tool for the analysis and interpretation of the obtained results. We would like to emphasize that the final goal of computational physics is not to reproduce some complex experimental trend. The final goal is to understand it and to come up with some transparent explanation. From this point of view, the realistic modeling will continue to play an important role, as a convenient tool for the analysis and interpretation of results of complex calculations.

Finally, the construction of the low-energy model is always conjugated with some approximations (and, as a matter of fact, the form of the model itself is the main approximation). However, we would like to emphasize from the very beginning that apart from these approximations, we do not use any adjustable parameters. Instead, the realistic modeling brings the state of the discussion to a qualitatively new level: if the model does not work, we need to reconsider the approximations underlying the definition of the model parameters or maybe the model itself.

2 Construction of multiorbital Hubbard model for the low-energy states

The first step of realistic modeling is the construction of an effective multiorbital Hubbard model in the low-energy part of spectrum:

$$\hat{\mathcal{H}} = \sum_{ij} \sum_{\alpha\beta} t_{ij}^{\alpha\beta} \hat{c}_{i\alpha}^\dagger \hat{c}_{j\beta} + \frac{1}{2} \sum_i \sum_{\alpha\beta\gamma\delta} U_{\alpha\beta\gamma\delta} \hat{c}_{i\alpha}^\dagger \hat{c}_{i\gamma}^\dagger \hat{c}_{i\beta} \hat{c}_{i\delta}, \quad (1)$$

which is regarded as the basic model in the physics of strongly correlated systems. Other models can be derived by considering some limiting cases of (1) (an example of the Heisenberg model will be considered in the next section). The Hubbard model is specified in the basis of Wannier orbitals, which are denoted by Greek symbols, each of which is a combination of spin ($s = \uparrow$ or \downarrow) and orbital (m) variables. The site-diagonal part of \hat{t}_{ij} describes the crystal-field splitting of the atomic levels, while the off-diagonal ($i \neq j$) elements stand for transfer integrals. If the relativistic spin-orbit interaction is not included, \hat{t}_{ij} is diagonal with respect to the spin indices. $U_{\alpha\beta\gamma\delta}$ are the matrix elements of screened Coulomb interactions for the low-energy states.

The most straightforward way to derive $\|\hat{t}_{ij}\|$ and $\|U_{\alpha\beta\gamma\delta}\|$ is to use a complete basis of localized orbitals in the low-energy part of spectrum. By the definition, this is the basis of Wannier functions [7]. There is a number of modern techniques, which can be used for the construction of Wannier functions, starting from one-electron Kohn-Sham orbitals in LDA. In the basis of localized pseudoatomic orbitals, which are used for example in the linear muffin-tin orbital (LMTO) method [6], it is convenient to use the projector-operator technique [8]. In the plane-wave basis, the Wannier functions can be constructed by minimizing the matrix elements of some local operators, such as the square of the position operator [9].

Then, the one-electron part $\|\hat{t}_{ij}\|$ of the Hubbard model (1) is identified with the matrix elements of the Kohn-Sham Hamiltonian in the basis of Wannier functions.¹

¹ Indeed, the Kohn-Sham Hamiltonian is also one-electron one. Moreover, since the exchange correlation potential in LDA is local, it does not contribute to the matrix elements between different atomic sites, so that the latter can be identified with the kinetic transfer integrals. Meanwhile, the site-diagonal contributions of the LDA potential to $\|\hat{t}_{ij}\|$ should be subtracted,

Since the Wannier basis is complete in the low-energy part of spectrum, the construction is exact, and the one-electron energies derived from $\|\hat{t}_{ij}\|$ coincide with the eigenenergies of the original LDA Hamiltonian (Fig. 1). Historically, the derivation of $\|\hat{t}_{ij}\|$ was based on the downfolding technique [10]. However, after some modifications, aiming to get rid of the frequency-dependence of \hat{t}_{ij} , this approach becomes equivalent to the projector-operator technique [8].

The effective Coulomb interaction in solids is defined as the energy cost for transferring an electron from one atomic site to another:

$$2(d^n) \rightleftharpoons d^{n+1} + d^{n-1}. \quad (2)$$

Even if such redistribution of electrons occurs in the low-energy part of spectrum (between appropriate Wannier orbitals), the corresponding change of the electron density can interact with the other electrons and change the electronic structure in the entire range of both low-energy and high-energy states. The change of the electronic structure in the high-energy part contributes to the screening of Coulomb interactions $\|U_{\alpha\beta\gamma\delta}\|$ in the low-energy part. Some of these effects can be described in the framework of the random-phase approximation (RPA) [11], which takes into account the screening of $U_{\alpha\beta\gamma\delta}$ due to the deformation of the Kohn-Sham orbitals in the course of the reaction (2).

Somewhat heuristically, in the pseudoatomic basis, the screening of Coulomb interactions, associated with the reaction (2), can be divided in two parts [10, 12]:

1. the screening, caused by relaxation of the pseudoatomic (basis) orbitals;
2. the self-screening of the low-energy states by the atomic states of the same origin, which contribute to other parts of spectrum due to the hybridization (the typical example is the screening of the t_{2g} -bands of the $3d$ -origin by the oxygen- and e_g -bands, which have a large weight of the atomic $3d$ -states due to the hybridization effects – see Fig. 1).

These two channels of screening can be easily incorporated in the framework of the constrained density-functional theory (DFT) and RPA, respectively [10]. Such a separation considerably facilitates the calculations and makes them more transparent.

3 Solution of the model Hamiltonian

The simplest way to solve the many-body problem (1) is to use the mean-field Hartree-Fock (HF) approach, where the ground-state wavefunction is approximated by the single Slater determinant, constructed from the one-electron orbitals $\{\phi_k\}$. The latter are obtained from the solution of the one-electron equations (in the reciprocal space):

$$(\hat{t}_{\mathbf{k}} + \hat{\mathcal{V}}) |\varphi_k\rangle = \varepsilon_k |\varphi_k\rangle, \quad (3)$$

where $\hat{t}_{\mathbf{k}}$ is the Fourier image of \hat{t}_{ij} , k is a collective index combining the momentum \mathbf{k} of the first Brillouin zone, the band number, and the spin ($s = \uparrow$ or \downarrow) of the particle, and $\hat{\mathcal{V}}$ is the HF potential

$$\mathcal{V}_{\alpha\beta} = \sum_{\gamma\delta} (U_{\alpha\beta\gamma\delta} - U_{\alpha\delta\gamma\beta}) n_{\gamma\delta}, \quad (4)$$

because the splitting of the atomic levels caused by electron-electron interactions is explicitly included in the second part of the Hubbard model [12].

expressed through the density matrix

$$\hat{n} \equiv \|n_{\gamma\delta}\| = \sum_k^{occ} |\varphi_k\rangle\langle\varphi_k|.$$

The latter is obtained self-consistently. By knowing $\{\phi_k\}$ and $\{\varepsilon_k\}$, it is easy to construct the one-electron (retarded) Green function $\hat{\mathcal{G}}_{ij}^{\uparrow,\downarrow}(\omega)$ for the spin \uparrow and \downarrow , which can be used in many applications. Particularly, one useful application is related to the analysis of interatomic magnetic interactions, which describe infinitesimal rotations of the spins near different magnetic equilibriums [13]. In this case, the total energy change can be mapped onto the Heisenberg model

$$E_{\text{Heis}} = -\frac{1}{2} \sum_{ij} J_{ij} \mathbf{e}_i \cdot \mathbf{e}_j \quad (5)$$

(\mathbf{e}_i and \mathbf{e}_j being the *directions* of the spin moments), and the parameters are given by

$$J_{ij} = \frac{1}{2\pi} \text{Im} \int_{-\infty}^{\varepsilon_F} d\omega \text{Tr}_L \left\{ \hat{\mathcal{G}}_{ij}^{\uparrow}(\omega) \Delta \hat{\mathcal{V}} \hat{\mathcal{G}}_{ji}^{\downarrow}(\omega) \Delta \hat{\mathcal{V}} \right\}. \quad (6)$$

In these notations, $\Delta \hat{\mathcal{V}} = \text{Tr}_S \{\hat{\sigma}_z \hat{\mathcal{V}}\}$ is the spin part of the Hartree-Fock potential, Tr_S (Tr_L) denotes the trace over the spin (orbital) indices, and $\hat{\sigma}_z$ is the Pauli matrix.²

The simplest way to go beyond the HF approximation is to consider the regular perturbation theory for correlation interactions. The latter are defined as the difference between true operator of electron-electron interactions in the Hubbard model (1) and its counterpart in the HF approximation (i.e., the combination of Coulomb and exchange interactions):

$$\hat{\mathcal{H}}_C = \sum_i \left(\frac{1}{2} \sum_{\alpha\beta\gamma\delta} U_{\alpha\beta\gamma\delta} \hat{c}_{i\alpha}^\dagger \hat{c}_{i\gamma}^\dagger \hat{c}_{i\beta} \hat{c}_{i\delta} - \sum_{\alpha\beta} \mathcal{V}_{\alpha\beta} \hat{c}_{i\alpha}^\dagger \hat{c}_{i\beta} \right). \quad (7)$$

For instance, in the second order, the correlation energy is given by:

$$E_C^{(2)} = - \sum_S \frac{\langle G | \hat{\mathcal{H}}_C | S \rangle \langle S | \hat{\mathcal{H}}_C | G \rangle}{E_{\text{HF}}(S) - E_{\text{HF}}(G)}, \quad (8)$$

where $|G\rangle$ is the ground-state wavefunction in the HF approximation and $|S\rangle$ is the excited state, which is obtained from $|G\rangle$ by replacing two orbitals in the occupied part of spectrum by two unoccupied orbitals.

Of course, this strategy is not universe. Nevertheless, it can be justified when the degeneracy of the ground state is already lifted (for instance, by the lattice distortions), so that the ground state can be described reasonably well by the single Slater determinant in the HF approximation and the correlation interactions can be included after that by considering the regular (non-degenerate) perturbation theory expansion.

In principle, one can go beyond the second order and consider higher-order effects for correlations interactions in the framework of the T-matrix theory [14,15].

² More precisely, the parameters J_{ij} in (6) define the *local* stability of the given magnetic configuration, which is stable if $J_{ij} > 0$ and unstable if $J_{ij} < 0$. In order to be consistent with the *global* definition of the parameters of the Heisenberg model (5), they should be additionally multiplied by $\mathbf{e}_i \cdot \mathbf{e}_j = 1$ and -1 , correspondingly for the ferromagnetic and antiferromagnetic bonds.

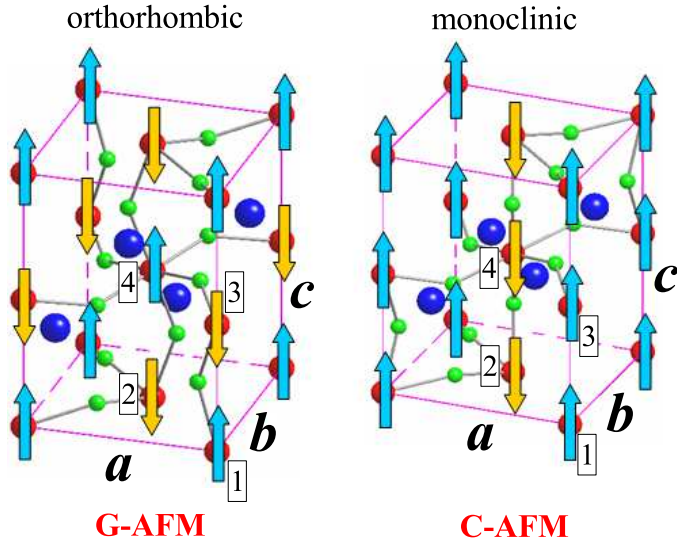


Fig. 2 G- and C-type antiferromagnetic ordering realized in the orthorhombic and monoclinic structure of YVO_3 .

4 Applications to vanadates $R\text{VO}_3$ ($R = \text{La, Ce, Pr, Nd, Sm, Gd, Tb, Yb, and Y}$)

The vanadates $R\text{VO}_3$ have attracted a considerable experimental and theoretical attention. All these compounds crystallize in the highly distorted perovskite structure. However, even small change of the crystal structure in $R\text{VO}_3$ can lead to dramatic change of the magnetic structure. Thus, this behavior can be regarded as a prototype of the “switching phenomena”. Below the magnetic transition temperature, the crystal structure of $R\text{VO}_3$ can be either orthorhombic (the space group D_{2h}^{16}) or monoclinic (the space group C_{2h}^5). The orthorhombic structure typically coexists with the G-type antiferromagnetic (AFM) ordering (Fig. 2), where all nearest-neighbor V-sites are coupled antiferromagnetically, while the monoclinic structure coexists with the C-type AFM ordering (ferromagnetic chains propagating along the c -axis and antiferromagnetically coupled in the ab -plane).

Depending on the size of the R^{3+} ions, which control the magnitude of the lattice distortion (particularly, the angles V-O-V, etc.), one can distinguish three types of behavior of $R\text{VO}_3$:

1. The materials containing large ions, such as La^{3+} , Ce^{3+} , Pr^{3+} , and Nd^{3+} , below the magnetic transition point crystallize in the monoclinic structure and develop the C-type AFM ordering. The transition to the orthorhombic phase typically occurs right above the Néel temperature (T_N) [16,17];
2. The low-temperature properties of $R\text{VO}_3$ with $R = \text{Sm, Gd, and Tb}$ are marked by a coexistence of orthorhombic and monoclinic phases. The monoclinic phase is formed above T_N . The orthorhombic phase starts to develop near magnetic transition and its proportion gradually increases with decreasing temperature [18,19,

20]. For example, at $T=5$ K, the proportion of the orthorhombic fraction is 25 % in SmVO_3 [18] and about 70 % in GdVO_3 [20].

3. In YVO_3 , the monoclinic structure is also formed well above $T_N=116$ K. With decreasing temperature, first C-type AFM ordering develops below T_N , within given monoclinic symmetry. Then, at $T_s=77$ K the crystal structure suddenly changes to the orthorhombic one. The corresponding magnetic structure also changes from C- to G-type AFM [21]. Similar behavior is observed in YbVO_3 .

Details of the experimental crystal structure and the magnetic properties of $R\text{VO}_3$ can be found in [16,17,18,19,21]. In the present work, we will use distorted vanadates in order to illustrate the main ideas of realistic modeling. There are several reasons why we have selected $R\text{VO}_3$ for these purposes:

1. The microscopic origin of two magnetic structures, which are realized in $R\text{VO}_3$, is still under debates. Although main details of the magnetic structures can be ascribed to the lattice distortions, which restrict the variation of the orbital degrees of freedom near some particular configurations [22,23], the role of orbital fluctuations away from these configurations is also actively discussed in the literature [24]. Particularly, the magnetic interactions in these systems are organized in such a way that the spin degrees of freedom are tightly coupled to the orbital ones, where any change of the orbital configuration affects the magnetic structure and vice versa. In the present work, we will illustrate how the computational tools, introduced in Sec. 3, can be used for the analysis of these properties.
2. The vanadates $R\text{VO}_3$ are currently regarded as some test compounds for various theories aiming to describe the close interplay among spin, orbital, and lattice degrees of freedom. Therefore, it is very important to test the ideas of realistic modeling on these systems and to apply them to the whole series of compounds $R\text{VO}_3$ with different R . All previous studies were mainly limited by LaVO_3 and YVO_3 [12,22,23,25].
3. We will also use $R\text{VO}_3$ in order to discuss some prototypical examples of the “switching phenomena”, which could be important in applications. Particularly, we will show how the magnetic structure of $R\text{VO}_3$ can be switched by changing the lattice distortions. An interesting example of switching between different spin and orbital states in $R\text{VO}_3$ by optical pulses was considered recently in [20, 26,27]. Another interesting example is the “magnetic field switching”, realized in DyVO_3 [28].

4.1 Parameters of the model Hamiltonian

In all the applications, the model was constructed for the t_{2g} -bands, located near the Fermi level (see Fig. 1).³ In vanadates $R\text{VO}_3$, each of V-site donates two electrons to these bands.

The first important set of parameters is related to the crystal field (CF), which is specified by the site-diagonal elements \hat{t}_{ii} of the one-electron Hamiltonian. It breaks the degeneracy of the atomic levels and define the type of occupied t_{2g} -orbitals in the atomic limit. The interactions, which may act against the crystal field and deform

³ We did not consider the magnetic effects associated with the rare-earth $4f$ -states, which can be also interesting and important [33]. It could be a good subject for a separate study, but in the present work, the $4f$ -states were treated as non-polarized quasiautomatic core states.

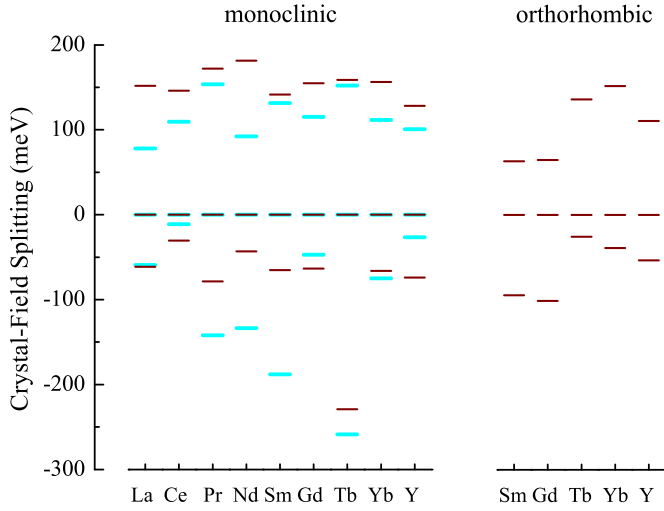


Fig. 3 The crystal-field splitting of three t_{2g} -levels in monoclinic (left) and orthorhombic (right) phases of RVO_3 . The energies are measured relative to the middle level, corresponding to the highest occupied orbital in the atomic limit. The splitting for two vanadium sublattices in the monoclinic phase is shown by different colors, where parameters for the less distorted sublattice (according to the energy difference between middle and highest orbitals) are denoted by the light blue color, while the ones for the more distorted sublattice – by the dark brown color.

the occupied orbitals are controlled by the intraatomic Coulomb repulsion \mathcal{U} , Hund’s rule coupling \mathcal{J} and transfer integrals \hat{t}_{ij} between different atomic sites. They will be discussed below.

The scheme of the t_{2g} -level splitting, obtained from the diagonalization of \hat{t}_{ii} , is shown in Fig. 3. The physically relevant parameter is the splitting between middle and highest orbitals (corresponding to the highest occupied and lowest unoccupied orbitals in the atomic limit). In the most cases this splitting is at least 100 meV. Somewhat exceptional behavior is observed in the monoclinic phase of $LaVO_3$ and in the orthorhombic phases of $SmVO_3$ and $GdVO_3$, where the characteristic splitting can be as small as 60-80 meV. Some consequences of this behavior will be discussed below. In the monoclinic phase, the splitting can be very different in two inequivalent V-sublattices, which are denoted as (1,2) and (3,4) in Fig. 2. For example, in $LaVO_3$ this splitting is 78 meV and 152 meV, respectively. An example of the CF-orbitals, obtained after the diagonalization of \hat{t}_{ii} for $SmVO_3$, is presented in Table 1.

An example of the transfer integrals in the local coordinate frame, corresponding to the diagonal representation of the crystal field at each atomic site, is shown in Table 2 for $SmVO_3$. The form of these integrals is very different from the one expected for the undistorted cubic structure.⁴ Thus, the crystal distortions have a profound effect not only on the t_{2g} -level splitting, but also on the form of the transfer integrals. All these details are very important for the analysis of the low-energy properties of vanadates.

⁴ In the cubic structure, the hoppings are allowed only between alike orbitals, lying in the plane of the bond. For example, in the z -direction, the hoppings can take place only between t_{2g} -orbitals of either yz or zx symmetry [29].

Table 1 Eigenenergies (measured in meV from the middle level) and eigenvectors obtained from the diagonalization of the crystal-field Hamiltonian \hat{t}_{ii} for orthorhombic ('o') and monoclinic ('m') phases of SmVO₃. The eigenvectors are expanded over the basis of xy , yz , z^2 , zx , and x^2-y^2 Wannier-orbitals, in the orthorhombic coordinate frame. Positions of atomic sites are explained in Fig. 2. The eigenvectors for other sites can be obtained using symmetry operations.

phase	site	energies	orbitals
'o'	1	-95	0, 0.22, -0.39, 0.84, 0.30
		0	0.06, 0.78, 0.22, -0.28, 0.51
		63	0.32, 0.52, 0.06, 0.17, -0.77
'm'	1	-65	-0.07, 0.70, 0.30, 0.63, -0.14
		0	-0.37, -0.05, 0.03, 0.20, 0.91
		142	0.12, 0.62, 0.18, -0.72, 0.23
'm'	3	-188	-0.39, 0.02, 0.04, 0.05, 0.92
		0	0.12, -0.87, 0.30, 0.37, 0.04
		132	0.20, 0.34, -0.21, 0.89, 0.04

Table 2 Transfer integrals (measured in meV) between nearest neighbors in the orthorhombic ('o') and monoclinic ('m') phases of SmVO₃ in the local coordinate frame corresponding to the diagonal representation of the crystal field. Positions of atomic sites are explained in Fig. 2.

phase	\hat{t}_{12}	\hat{t}_{34}	\hat{t}_{13}
'o'	$\begin{pmatrix} 69 & 157 & 4 \\ 2 & -86 & -94 \\ 25 & 25 & -123 \end{pmatrix}$	$\begin{pmatrix} 69 & 157 & 4 \\ 2 & -86 & -94 \\ 25 & 25 & -123 \end{pmatrix}$	$\begin{pmatrix} 86 & -53 & -4 \\ -53 & 56 & -64 \\ -4 & -64 & 12 \end{pmatrix}$
'm'	$\begin{pmatrix} 42 & -29 & -142 \\ -36 & -118 & -40 \\ -5 & 23 & -43 \end{pmatrix}$	$\begin{pmatrix} -121 & -43 & -24 \\ 41 & 22 & -12 \\ -19 & -124 & -10 \end{pmatrix}$	$\begin{pmatrix} 54 & 23 & -155 \\ 15 & -25 & 74 \\ -21 & -139 & -102 \end{pmatrix}$

Without help of the first-principles electronic structure calculations, it is practically impossible to fix all the parameters in an unambiguous manner.

The behavior of screened Coulomb and exchange interactions in the t_{2g} -band is illustrated in Fig. 4. For these (purely explanatory) purposes, the whole matrices of screened Coulomb interactions were fitted in terms of two Kanamori parameters [14]: the intraorbital Coulomb interaction \mathcal{U} and the exchange interaction \mathcal{J} .⁵ The Coulomb interaction \mathcal{U} is slightly larger than 3 eV and somewhat sensitive to the local environment of the V-sites in solids. In orthorhombic systems, \mathcal{U} increases with the lattice distortion in the direction Sm→Y. In monoclinic systems, this dependence is not so obvious. Also in the monoclinic systems, the values of \mathcal{U} are slightly different for the inequivalent V-sublattices. On the other hand, the screening of the exchange interaction \mathcal{J} is practically insensitive to the local environment, and for all considered compounds \mathcal{J} is close to 0.62 eV.

Another important parameter, which controls the orbital state and can compete with the CF splitting, is the energy gain caused by the superexchange (SE) processes: $\text{Tr}_L(\hat{t}_{ij}\hat{t}_{ji})/(\mathcal{U}-3\mathcal{J})$ and $\text{Tr}_L(\hat{t}_{ij}\hat{t}_{ji})/\mathcal{U}$, correspondingly for the ferromagnetically and antiferromagnetically coupled bonds [30]. Using the values of transfer integrals between nearest neighbors (Table 2), Coulomb \mathcal{U} and exchange \mathcal{J} interactions (Fig. 4), this

⁵ For third Kanamori parameter – the interorbital Coulomb interaction \mathcal{U}' – we used the relation $\mathcal{U}' = \mathcal{U} - 2\mathcal{J}$, which holds for the t_{2g} -states in the cubic environment.

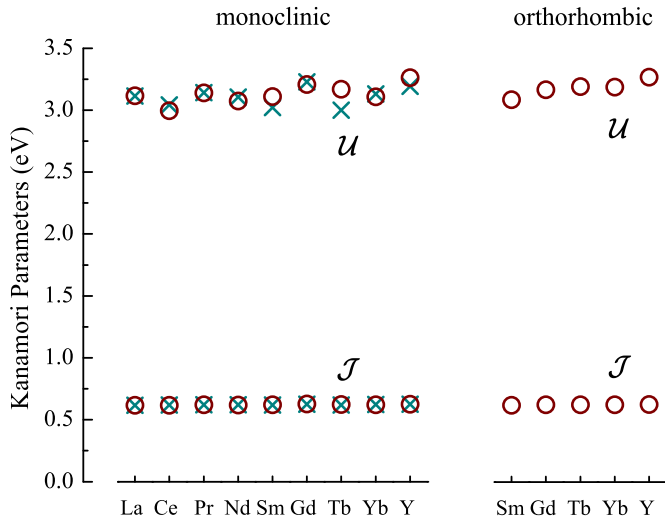


Fig. 4 Parameters of screened intraorbital Coulomb interaction \mathcal{U} and the exchange interaction \mathcal{J} derived for the t_{2g} -bands of RVO_3 in monoclinic (left) and orthorhombic (right) phase. The parameters for two different V-sublattices in the monoclinic phase are shown by different symbols: the values corresponding to the more distorted environment (according to the scheme of the crystal-field splitting in Fig. 3) are shown by circles, while the values corresponding to the less distorted environment are shown by crosses.

energy gain can be estimated (very roughly) as 7-40 meV per one V-V bond. Thus, the energy gain caused by the SE processes is expected to be smaller or at least comparable with the CF splitting (Fig. 3).⁶ Thus, there is no predominant mechanism and both crystal field and SE processes can play some role in the formation of the orbital (and related to it magnetic) ground state of vanadates RVO_3 . More detailed analysis will be given in the next sections.

4.2 Relative stability of magnetic structures: total energies

In this section we will discuss abilities of theories, which implies that the orbital degrees of freedom are frozen in some peculiar configuration by the lattice distortions, and the magnetic structure simply follow them, basically according to the conventional Goodenough-Kanamori [31,32].⁷

A typical example of the orbital ordering is shown in Fig. 5 for $TbVO_3$. We have selected this material because it has the largest CF splitting (Fig. 3) and therefore it

⁶ Note that since each V-site participate in six bonds, the energy gain recalculated “per site” will be larger. On the other hand, the simple estimates in this section do not take into account the Pauli principle, which forbids the hoppings onto already occupied orbitals and makes energy gain smaller. Thus, this is indeed only an “order or magnitude estimate”.

⁷ In the present contents, the “Goodenough-Kanamori rules” means that the maximal overlap between occupied orbitals in some particular bond favors AFM interactions, while the minimal overlap between occupied orbitals (or the maximal overlap between occupied and unoccupied orbitals) favors FM interactions.

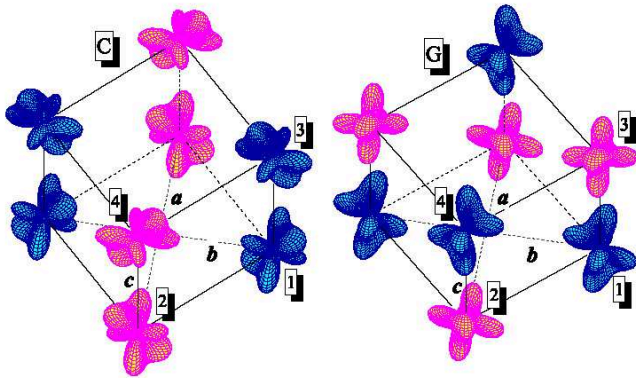


Fig. 5 Distribution of charge densities associated with occupied t_{2g} -orbitals (the orbital ordering) realized in the monoclinic (left) and orthorhombic (right) phases of TbVO_3 in the Hartree-Fock approximation. Different magnetic sublattices associated with opposite directions of spins in the C- (left) and G- (right) type antiferromagnetic ground state are shown by different colors.

is the most appropriate for the analysis in the present contents. In the orthorhombic phase of TbVO_3 , the occupied orbitals have a large overlap in all three directions. Therefore, it is reasonable to expect the AFM character of interactions and the G-type AFM ground state. In the monoclinic phase, the overlap between occupied orbitals along the c -axis is considerably weaker. Thus, this orbital configuration will favor FM character of interactions in the c -direction and the C-type AFM ground state.

Another important point of the CF theory is that as long as the orbitals degeneracy is lifted by the lattice distortions, there is a hope that the correct magnetic ground state can be reproduced already at the level of the HF approximation. In some sense, the situation is similar to the closed atomic shell, where the ground state is also non-degenerate and can be described by the single Slater determinant. Then, if necessary, the correlation interactions can be taken into account on the top of the HF approximation, using regular perturbation theory expansion.

All these trends are clearly seen in the total energy calculations for the $R\text{VO}_3$ ($R=\text{La-Nd}$) compounds, which below the magnetic transition temperature stabilize in only one – monoclinic structure. Fig. 6 shows the behavior of stabilization energy (minus total energy measured relative to the FM state) for the AFM configurations of the A-, C-, and G-type.⁸ We note the following:

1. The HF approximation predicts the correct C-type AFM ground state for all four compounds;
2. The correlation interactions, which were taken into account using regular perturbation theory expansion near the HF solution for each magnetic state, additionally stabilize the experimentally observed C-type AFM ordering. Moreover, both second order perturbation and the T-matrix theory provide very consistent explanation for the behavior of correlation energies, although the energies obtained in the T-matrix

⁸ The C- and G-type AFM structures are explained in Fig. 2. The A-type AFM structure consists of the FM \mathbf{ab} -planes, which are coupled antiferromagnetically along the c -axis.

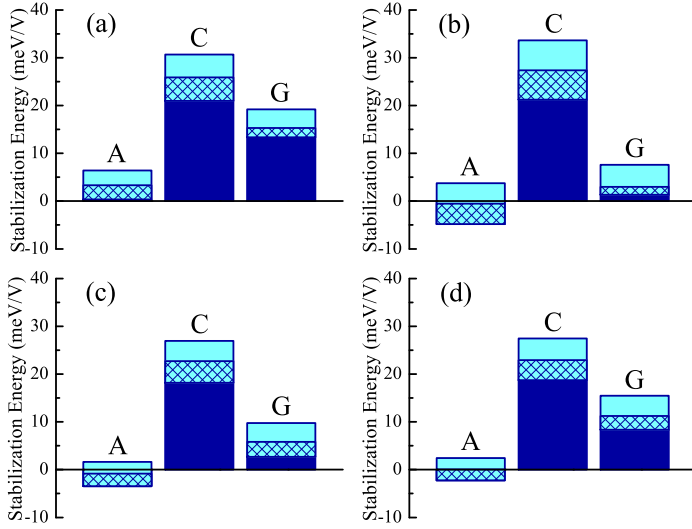


Fig. 6 Stabilization energies of the main antiferromagnetic states in LaVO_3 (a), CeVO_3 (b), PrVO_3 (c), and NdVO_3 (d) measured relative to the ferromagnetic state as obtained in the Hartree-Fock approximation (dark blue area) and after taking into account the correlation interactions in the second order of perturbation theory (light blue area) and in the framework of the T-matrix theory (hatched area).

theory for the AFM states are systematically smaller due to the higher-order correlation effects, which are included to the T-matrix, but not to the second-order perturbation theory.

Thus, not only the one-electron crystal field, which break the degeneracy of the HF states in some peculiar way, but also the correlation interactions play an important role in stabilizing the experimentally observed C-type AFM ordering in compounds $R\text{VO}_3$ ($R = \text{La-Nd}$). The stabilization energies of the correlation origin are systematically larger for the C-type AFM state, irrespectively on the approximation employed for treating the correlation interactions.

How general are these results?

Let us consider the next group of compounds $R\text{VO}_3$ ($R = \text{Sm, Gd, and Tb}$), which below the magnetic transition temperature exist *simultaneously* in the monoclinic and orthorhombic phases. The experimental crystal structure parameters, which have been refined for both phases, can be found in [18,19]. In the present study we use the data for $T = 5$ K. The stabilization energies for several AFM states, calculated for two crystallographic modifications, are shown in Fig. 7. Their behavior is quite consistent with the expectations based on the simplified CF theory: the monoclinic structure tends to stabilize the C-type AFM ordering, while the orthorhombic structure – G-type AFM ordering, although with some exceptions. For example, in the orthorhombic phase of SmVO_3 , the total energy is lower for the C-type AFM state, although the next G-type AFM state is very close in energy (the energy difference between G- and C-type AFM states is only 0.8 meV per one V-site). It seems that the quasidegeneracy of the G- and C-type AFM states is the generic feature of SmVO_3 and GdVO_3 (but not of TbVO_3). In the monoclinic phase of GdVO_3 , the C-type AFM state has the lowest energy. However, the next G-type AFM state is only 1.4 meV higher than the C-type

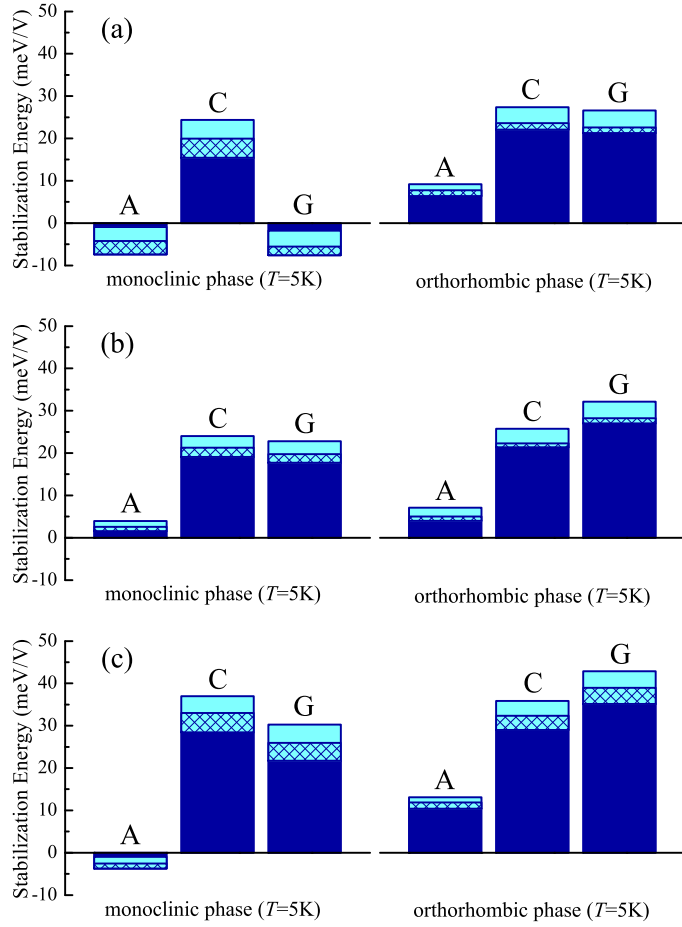


Fig. 7 Stabilization energies of the main antiferromagnetic states in SmVO₃ (a), GdVO₃ (b), and TbVO₃ (d) relative to the ferromagnetic state as obtained in the Hartree-Fock approximation (dark blue area) and after taking into account the correlation interactions in the second order of perturbation theory (light blue area) and in the framework of the T-matrix theory (hatched area). Results for the orthorhombic and monoclinic phases (obtained using the experimental crystal structure at $T=5$ K) are shown correspondingly in the left and right parts of the figure.

AFM state. This picture seems to be consistent with the experimentally observed phase coexistence, which means that there should be several phases competing in a narrow energy range. For example, the proximity of G- and C-type AFM states in one of the crystallographic phases may indicate at the importance of magnetic forces in driving the transition to another phase. More specifically, in SmVO₃ at $T=5$ K, the smaller orthorhombic fraction ($\sim 25\%$ of the volume [18]) should be nearly unstable, because the magnetic transition to the C-type AFM state can cause the structural transition. On the contrary, in GdVO₃ the smaller volume fraction is monoclinic ($\sim 30\%$ at $T=5$ K [20]), which is also nearly unstable, because the change of the crystal structure in this case can be induced by the magnetic transition to the G-type AFM state. Such a

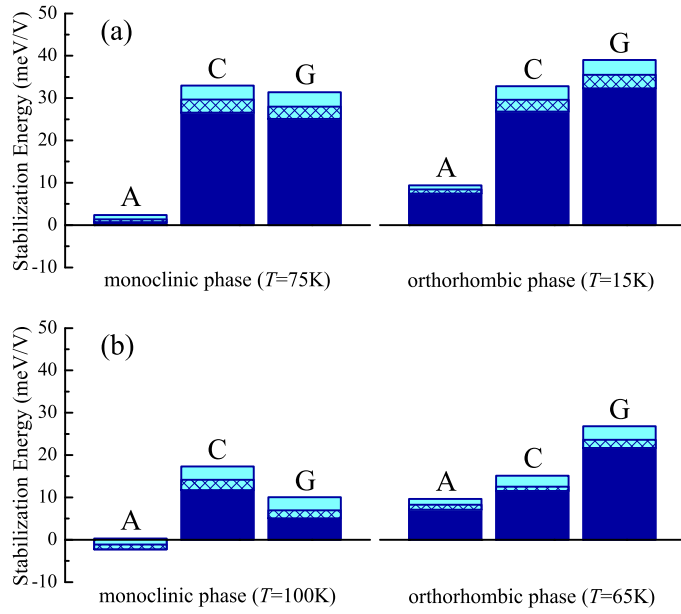


Fig. 8 Stabilization energies of the main antiferromagnetic states in YbVO₃ (a) and YVO₃ (b) relative to the ferromagnetic state as obtained in the Hartree-Fock approximation (dark blue area) and after taking into account the correlation interactions in the second order of perturbation theory (light blue area) and in the framework of the T-matrix theory (hatched area). Results for the orthorhombic and monoclinic phases are shown correspondingly in the left and right part of the figure.

transition can be caused either by the exchange striction (basically, the change of the lattice parameters associated with the change of the magnetic state) or by the change of the orbital structure, which would further minimize the energy of SE interactions [30]. The relative role of these two mechanisms will be clarified in the next section. The quasidegeneracy of magnetic states in the monoclinic phase of GdVO₃ may be also resolved through the additional symmetry-breaking transition and emergence of a new ordered phase, as it was suggested in some experimental reports [20].

Similar to the previous group of compounds, the correlation interactions in RVO_3 ($R = \text{Sm, Gd, and Tb}$) play an important role and additionally stabilize the “correct” magnetic ground state: C-type AFM for monoclinic systems and G-type AFM for orthorhombic ones.

Typical representatives of the last group of compounds are YbVO₃ and YVO₃. Similar to the previous case, below the Néel temperature, YbVO₃ and YVO₃ can be found both in orthorhombic and monoclinic modifications. However, contrary to RVO_3 ($R = \text{Sm, Gd, and Tb}$), these two phases emerges *consequently*, in two different temperature intervals. For examples, below $T_s = 77$ K, YVO₃ crystallizes in the orthorhombic modification, and above T_s – in the monoclinic one. The construction and solution of the model Hamiltonian for YVO₃ have been discussed in details in [12, 15, 25]. Here we summarize the main results for the total energies. They are shown in Fig. 8 (together with YbVO₃, which exhibits quite a similar behavior). In this case, the type of the magnetic ground state realized in each temperature range is controlled by the crystals

structure: the low-temperature orthorhombic phase coexists with the G-type AFM ordering, while the high-temperature monoclinic phase coexists with the C-type AFM ordering. Each magnetic ground state can be reproduced at the level of the HF approximation and is additionally stabilized by correlation interactions, considered in the framework of the second-order perturbation theory as well as in the T-matrix theory.

4.3 Interatomic magnetic interactions as a probe of the orbital state

In this section we will discuss some limitations of the CF theories. Since the CF splitting is finite, the orbital degrees of freedom are not fully quenched and can be affected by other interactions, which generally compete with the crystal field. Particularly, another major factor “reshaping” the orbitals is related to the superexchange processes [30]. In this case, the occupied orbitals will tend to additionally adjust their form for each magnetic state by minimizing the energy of SE interactions. The magnitude of this effect is controlled by the ratio of $\text{Tr}_L(\hat{t}_{ij}\hat{t}_{ji})/\mathcal{U}$ to the CF splitting.

Thus, the main question, which will be addressed in this section is *how flexible are the orbital degrees of freedom in RVO_3* ? A very useful tool for the analysis of this kind of problem is the interatomic magnetic interactions (6). Since interatomic magnetic interactions are defined *locally*, via infinitesimal rotations of spins, they carry an information about the details of the orbital state in each magnetic state. Thus, the parameters of the Heisenberg model (5) depend on the magnetic state in which they are calculated. However, it is not an artifact of calculations or the Heisenberg model itself. This dependence has a clear physical meaning and reflects the changes of the orbital configuration in each magnetic state.

This effect is clearly seen in the behavior of nearest-neighbor magnetic interactions in RVO_3 ($R = \text{La, Ce, Pr, and Nd}$), crystallizing in the monoclinic structure (Fig. 9). Let us consider first the least distorted compound CeVO_3 (similar situation occurs in LaVO_3 , which was considered in [25]). Distribution of the charge densities associated with the occupied t_{2g} -orbitals (the so-called orbital ordering), which was obtained by minimizing the HF energy for different magnetic states, is shown in Fig. 10. This compound has two V-sublattices: “less distorted” (according to the values of the CF-splitting – Fig. 3) sublattice (1,2) and “more distorted” one (3,4). Then, one can see even visually that the shape of the orbitals changes depending on the magnetic state. As expected, the orbitals in the “less distorted” sublattice (1,2) are more flexible. The largest change of the occupied orbitals occurs in the G-type AFM state. All these tendencies are reflected in the behavior of interatomic magnetic interactions (Fig. 9), which tend to additionally stabilize the magnetic state in which they are calculated. Particularly, the FM interaction J_{13} decreases drastically in the G-type AFM state. On the other hand, the strength of the AFM interaction J_{12} increases. Similar situation occurs in LaVO_3 [25]: due to the rearrangement of the occupied orbitals, not only C-, but also G-type AFM state becomes locally stable (all nearest-neighbor interactions are antiferromagnetic in the G-type AFM state, while J_{12} is ferromagnetic in the C-type AFM state). Nevertheless, the C-type AFM state has lower energy and is realized as the true magnetic ground state of LaVO_3 (Fig. 6). Furthermore, the orbital ordering in the A-type AFM state of LaVO_3 further breaks the monoclinic symmetry and makes two inequivalent sublattices in the plane (1,2) (which is reflected in the splitting of each of the magnetic interaction J_{12} and J_{13} in two types – ferromagnetic and antiferromagnetic). When the crystal distortion increases in the direction LaVO_3

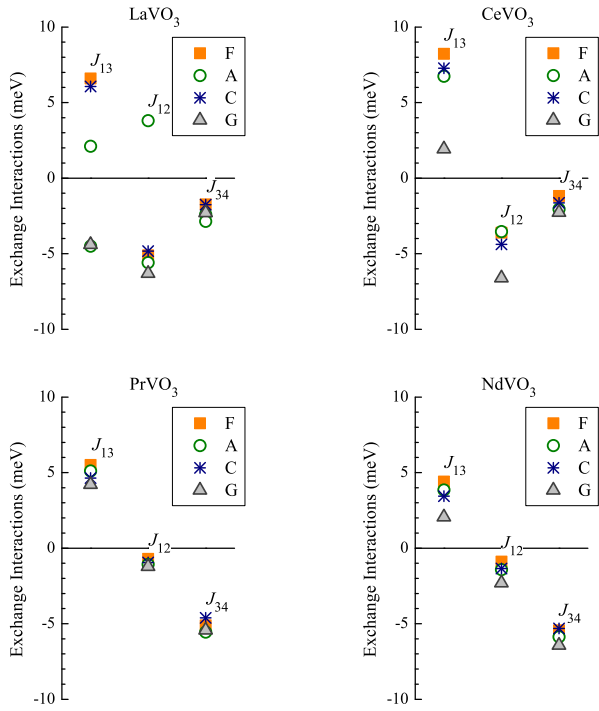


Fig. 9 Nearest-neighbor magnetic interactions in LaVO_3 , CeVO_3 , PrVO_3 , and NdVO_3 calculated in the ferromagnetic (F) and in the A-, C, and G-type antiferromagnetic states using the expression (6) for the infinitesimal rotations of spins.

$\rightarrow \text{CeVO}_3 \rightarrow \text{PrVO}_3 \rightarrow \text{NdVO}_3$ (see Fig. 3), the orbitals become less flexible, and the magnetic interactions in PrVO_3 and NdVO_3 only weakly depend on the magnetic state in which they are calculated. Thus, in the last two compounds, we have more or less conventional CF scenario of the orbital ordering and related to it interatomic magnetic interactions.

The behavior of interatomic magnetic interactions in $R\text{VO}_3$ ($R = \text{Sm}$, Gd , and Tb), crystallizing simultaneously in the monoclinic and orthorhombic structures, is explained in Fig. 11. As was pointed out in the previous section, one of the interesting features in this regime is the quasidegeneracy of the C- and G-type AFM states, realized in the orthorhombic phase of SmVO_3 and in the monoclinic phase of GdVO_3 . Therefore, we have to address the question whether this quasidegeneracy is related to the reconstruction of the orbitals ordering, which will further affect the interatomic magnetic interactions and make them specific for each magnetic state, or to some other effects, such as the exchange striction. The typical example of the orbital ordering realized in the orthorhombic phase of SmVO_3 is shown in Fig. 12. The orbital degrees of freedom in these compounds are indeed rather flexible and to some extent are able to adjust the change of the magnetic state. Nevertheless, one important aspect is that the orbital ordering does not significantly change between the C- and G-type AFM states. In fact, the orbital ordering pattern in the orthorhombic phase of SmVO_3 can be of two types: one type is realized for the C- and G-type AFM states and another type –

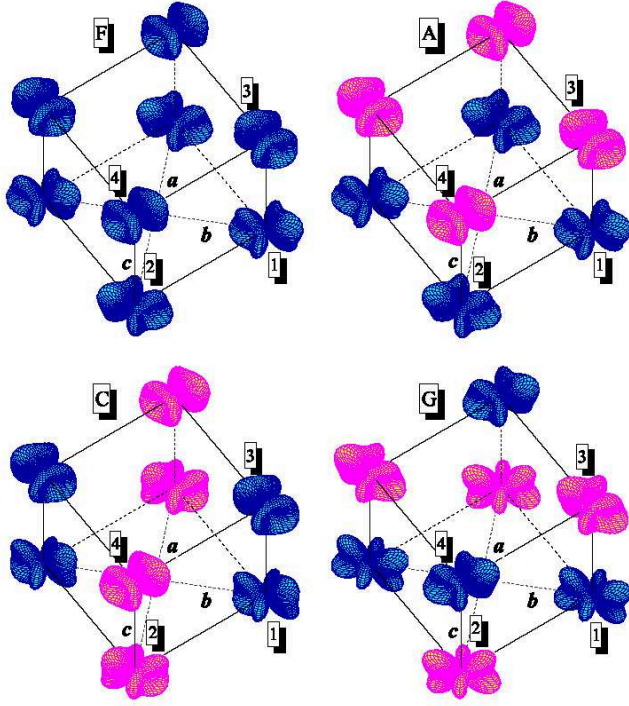


Fig. 10 Orbital ordering realized in the Hartree-Fock approximation for the ferromagnetic (F) and A-, C-, and G-type antiferromagnetic states of CeVO_3 . Different magnetic sublattices are shown by different colors.

for the F-state and the A-type AFM state. The orbital ordering within each group of states is practically identical. This behavior of the orbital degrees of freedom is reflected in the behavior of interatomic magnetic interactions (Fig. 11): similar to the orbital ordering, there are two sets of the parameters $\{J_{ij}\}$, one of which acts in the F- and A-states and another one – in the C- and G-states. The difference is mainly reflected in the behavior of in-plane interaction J_{12} . Similar situation occurs in the monoclinic phase of GdVO_3 , where two sets of the in-plane interactions J_{34} are associated with different orbital states, realized correspondingly for the FM and A-type AFM ordering and for the C- and G-type AFM ordering. Thus, the quasidegeneracy of the C- and G-type AFM states in SmVO_3 and GdVO_3 cannot be related to the change of the orbital state. A more likely scenario is the exchange striction, where the change of the lattice parameters can easily change the sign of the weak inter-plane interaction J_{13} .

The interatomic magnetic interactions for the last two compounds, YbVO_3 and YVO_3 , which exhibits the consecutive monoclinic-to-orthorhombic transition with the decrease of temperature are shown in Fig. 13. Details of the orbital ordering and interatomic magnetic interactions for YVO_3 can be found in [25]. In this case, the orbitals degrees of freedom can remain flexible and the interatomic magnetic interactions depend on the magnetic states (especially for the orthorhombic phase of YVO_3). Nevertheless, the effect is not so strong as in SmVO_3 and GdVO_3 . Moreover, the form of the

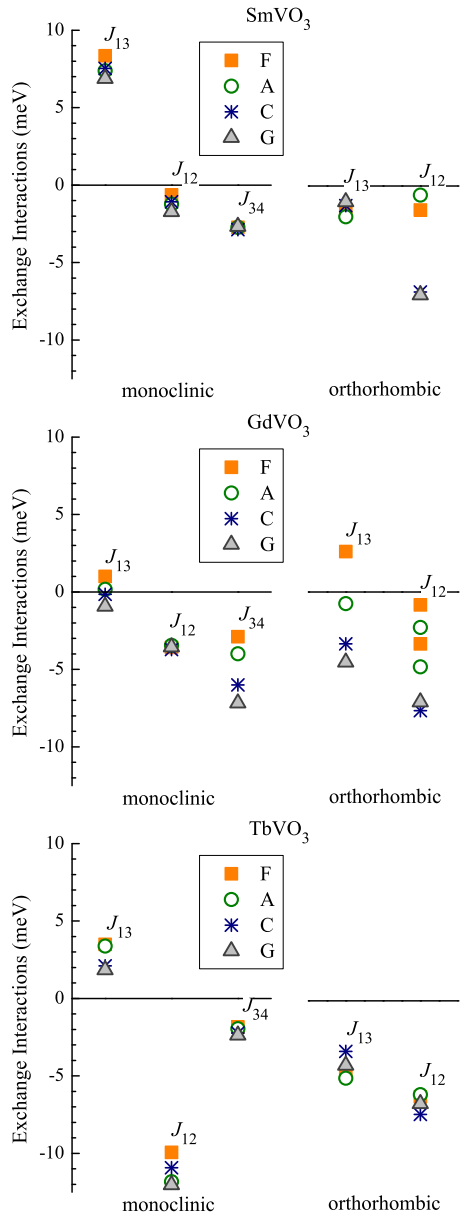


Fig. 11 Nearest-neighbor magnetic interactions in the monoclinic (left) and orthorhombic (right) phases of SmVO_3 , GdVO_3 , and TbVO_3 , calculated in the ferromagnetic (F) and in the A-, C, and G-type antiferromagnetic states using the expression (6) for the infinitesimal rotations of spins.

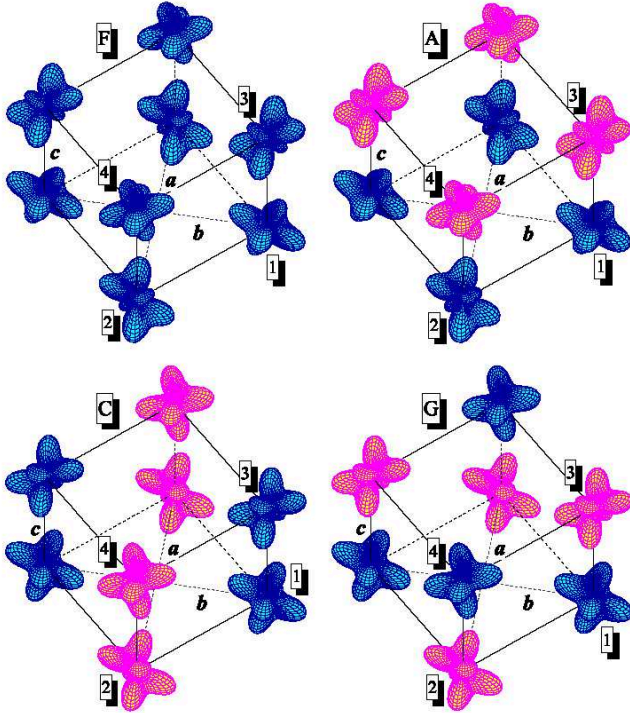


Fig. 12 Orbital ordering realized in the Hartree-Fock approximation for the ferromagnetic (F) and A-, C-, and G-type antiferromagnetic states of orthorhombic SmVO_3 (at $T = 5$ K). Different magnetic sublattices are shown by different colors.

orbital ordering and interatomic magnetic interactions, obtained for the C- and G-type AFM states in each of the crystallographic modification, is practically the same (similar to SmVO_3 and GdVO_3). Thus, the orbital fluctuations do not seem to be the trigger for the C-G-type AFM transition and the concomitant monoclinic-to-orthorhombic phase transition. The present results are more consistent with the scenario where the structural transition goes first, while the spin and orbital degrees of freedom mainly follow the change of the crystal structure.

5 Summary and Conclusions

We have reviewed the main ideas of realistic modeling of the strongly correlated systems. This is a new direction of the electronic structure calculations, which is especially suit for complex oxides materials. In the present context, the term “complex” means the computational complexity (the necessity to deal with highly distorted crystal structures having very low symmetry and many atoms in the unit cell) as well as the methodological complexity (the necessity to go beyond conventional approximations in the electronic structure calculations, such as the local-density approximation). The basic idea of realistic modeling is to construct an effective low-energy model for

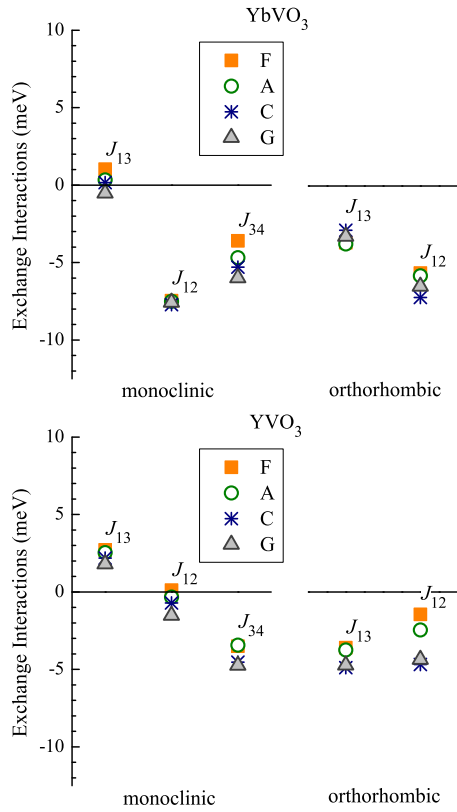


Fig. 13 Nearest-neighbor magnetic interactions in the monoclinic (left) and orthorhombic (right) phases of YbVO_3 and YVO_3 , calculated in the ferromagnetic (F) and in the A-, C-, and G-type antiferromagnetic states using the expression (6) for the infinitesimal rotations of spins.

the states close to the Fermi level, derive all the parameters rigorously, on the basis of first-principles electronic structure calculations, and to solve this model using modern many-body techniques. Thus, realistic modeling combines the accuracy and predictable power of first-principles electronic structure calculations with the flexibility and insights of the model analysis.

It is certainly true that approximations are inevitable in such an approach (and the form of the low-energy model itself is the main approximation!). However, we would like to emphasize again that apart from these approximations, the entire procedure is parameter-free. Namely, we do not need anymore to deal with numerous adjustable parameters. Instead, the state of the discussion is brought to a qualitatively new level: how to improve the approximations used for the definition and calculation of the model parameters.

The abilities of this method were demonstrated on the wide series of vanadates $R\text{VO}_3$ ($R = \text{La}, \text{Ce}, \text{Pr}, \text{Nd}, \text{Sm}, \text{Gd}, \text{Tb}, \text{Yb}, \text{and Y}$) with distorted perovskite structure. Particular attention was paid to computational tools, which can be used for the microscopic analysis of different spin and orbital states realized in the partially filled t_{2g} -band. Meanwhile, we were able to solve a number of fundamental and materialogical

problems related to the origin of the C- and G-type AFM states in these compounds. The first applications of realistic modeling are very encouraging. We hope that these ideas will continue to develop in the future to become a powerful tool for theoretical analysis of complex oxide materials and other strongly correlated systems.

Acknowledgements I am grateful to G.R. Blake for providing details of the experimental crystal structure for the series of compounds RVO_3 . I also wish to thank the support from the Federal Agency for Science and Innovations, grant No. 02.740.11.0217, during my stay at the Ural State Technical University (Ekaterinburg, Russia).

References

1. Norman, M.R.: High-temperature superconductivity in the iron pnictides. *Physics* **1**, 21 (2008)
2. Tokura, Y.: Critical features of colossal magnetoresistive manganites. *Rep. Prog. Phys.* **69**, 797 (2006)
3. Khomskii, D.: Classifying multiferroics: Mechanisms and effects. *Physics* **2**, 20 (2009)
4. Imada, M., Fujimori, A., Tokura, Y.: Metal-insulator transitions. *Rev. Mod. Phys.* **70**, 1039 (1998)
5. Kohn, W.: Nobel Lecture: Electronic structure of matter: wave functions and density functionals. *Rev. Mod. Phys.* **71**, 1253 (1999)
6. Andersen, O.K., Jepsen, O.: Explicit, First-Principles Tight-Binding Theory. *Phys. Rev. Lett.* **53**, 2571 (1984)
7. Wannier, G.H.: The Structure of Electronic Excitation Levels in Insulating Crystals. *Phys. Rev.* **52**, 191 (1937)
8. Solovyev, I.V., Pchelkina, Z.V., Anisimov, V.I.: Construction of Wannier functions from localized atomiclike orbitals. *Phys. Rev. B.* **75**, 045110 (2007)
9. Marzari, N., Vanderbilt, D.: Maximally localized generalized Wannier functions for composite energy bands. *Phys. Rev. B.* **56**, 12847 (1997)
10. Solovyev, I.V.: First-principles Wannier functions and effective lattice fermion models for narrow-band compounds. *Phys. Rev. B.* **73**, 155117 (2006)
11. Aryasetiawan, F., Imada, M., Georges, A., Kotliar, G., Biermann, S., Lichtenstein, A.I., Frequency-dependent local interactions and low-energy effective models from electronic structure calculations. *Phys. Rev. B.* **70**, 195104 (2004)
12. Solovyev, I.V.: Combining DFT and Many-Body Methods to Understand Correlated Materials. *J. Phys.: Condens. Matter* **20**, 293201 (2008)
13. Lichtenstein, A.I., Katsnelson, M.I., Antropov, V.P., Gubanov, V.A.: Local spin density functional approach to the theory of exchange interactions in ferromagnetic metals and alloys. *J. Magn. Magn. Matter.* **67**, 65 (1987)
14. Kanamori, J.: Electron Correlation and Ferromagnetism of Transition Metals. *Prog. Theor. Phys.* **30**, 275 (1963)
15. Solovyev, I.V.: Correlation Energies in Distorted $3d-t_{2g}$ Perovskite Oxides. *J. Exp. Theor. Phys.* **105**, 46 (2007)
16. Zubkov, V.G., Bazuev, G.V., Perelyaev, V.A., Shveikin, G.P.: Magnetic structure of $LaVO_3$. *Sov. Phys. Solid State* **15**, 1079 (1973)
17. Bordet, P., Chaillout, P., Marezio, M., Huang, Q., Santoro, A., Cheong, S.-W., Takagi, H., Oglesby, C.S., Batlogg, B.: Structural Aspects of the Crystallographic-Magnetic Transition in $LaVO_3$ around 140 K. *J. Solid State Chem.* **106**, 253 (1993)
18. Sage, M.H., Blake, G.R., Nieuwenhuys, G.J., Palstra, T.T.M.: Evidence for Electronic Phase Separation between Orbital Orderings in $SmVO_3$. *Phys. Rev. Lett.* **96**, 036401 (2006)
19. Sage, M.H., PhD Thesis "Orbital, charge and magnetic order of RVO_3 perovskites", 155. Print Partners Ipskamp B.V., Enschede, the Netherlands (2006)
20. Yusupov, R.V., Mihailovic, D., Colin, C.V., Blake, G.R., Palstra, T.T.M.: Critical phenomena and femtosecond ordering dynamics associated with electronic and spin-ordered phases in YVO_3 and $GdVO_3$. *Phys. Rev. B.* **81**, 075103 (2010)
21. Blake, G.R., Palstra, T.T.M., Ren, Y., Nugroho, A.A., Menovsky, A.A.: Neutron diffraction, x-ray diffraction, and specific heat studies of orbital ordering in YVO_3 . *Phys. Rev. B* **65**, 174112 (2002)

-
22. Sawada, H., Terakura, K.: Orbital and magnetic orderings in localized t_{2g} systems, YTiO_3 and YVO_3 : Comparison with a more itinerant e_g system LaMnO_3 . *Phys. Rev. B.* **58**, 6831 (1998)
 23. Fang, Z., Nagaosa, N.: Quantum Versus Jahn-Teller Orbital Physics in YVO_3 and LaVO_3 . *Phys. Rev. Lett.* **93**, 176404 (2004)
 24. Khaliullin, G.: Orbital Order and Fluctuations in Mott Insulators. *Prog. Theor. Phys. Suppl.* **160**, 155 (2005)
 25. Solovyev, I.V.: Lattice distortion and magnetism of $3d$ - t_{2g} perovskite oxides. *Phys. Rev. B.* **74**, 054412 (2006)
 26. Tomimoto, S., Miyazaka, S., Ogasawara, T., Okamoto, H., Tokura, Y.: Ultrafast photoinduced melting of orbital order in LaVO_3 . *Phys. Rev. B.* **68**, 035106 (2003)
 27. Mazurenko, D.A., Nugroho, A.A., Palstra, T.T.M., van Loosdrecht, P.H.M.: Dynamics of Spin and Orbital Phase Transitions in YVO_3 . *Phys. Rev. Lett.* **101**, 245702 (2008)
 28. Miyasaka, S., Yasue, T., Fujioka, J., Yamasaki, Y., Okimoto, Y., Kumai, R., Arima, T., Tokura, Y.: Magnetic Field Switching between the Two Orbital-Ordered States in DyVO_3 . *Phys. Rev. Lett.* **99**, 217201 (2007)
 29. Slater, J.C., Koster, G.F.: Simplified LCAO Method for the Periodic Potential Problem. *Phys. Rev.* **94**, 1498 (1954)
 30. Kugel, K.I., Khomskii, D.I.: The Jahn-Teller effect and magnetism: transition metal compounds. *Sov. Phys. Usp.* **25**, 231 (1982)
 31. Goodenough, J.B., *Magnetism and the Chemical Bond*, 394. Interscience, New York (1963)
 32. Kanamori, J.: Superexchange interaction and symmetry properties of electron orbitals. *J. Phys. Chem. Solids* **10**, 87 (1959)
 33. Reehuis, M., Ulrich, C., Pattison, P., Ouladdiaf, B., Rheinstädter, M.C., Ohl, M., Regnault, L.P., Miyasaka, M., Tokura, Y., Keimer, B.: Neutron diffraction study of YVO_3 , NdVO_3 , and TbVO_3 . *Phys. Rev. B.* **73**, 094440 (2006)